JOURNAL OF MATERIALS SCIENCE 11 (1976) 1227–1238

Decomposition of TiO_2-SnO_2 solid solutions

M. W. PARK, T. E. MITCHELL, A. H. HEUER
Department of Metallurgy and Materials Science, Case Western Reserve University, Cleveland, Ohio, USA

Decomposition of TiO_2–SnO_2 solid solutions was studied using large-angle X-ray diffraction, transmission electron microscopy, electron diffraction, and small-angle X-ray scattering. Particular attention was devoted to the initial stages of decomposition of homogeneous solid solutions, so as to determine whether or not decomposition in the system can occur spinodally. All of our results indicate that alloys within the spinodal can decompose by a continuous and spontaneous process, i.e. spinodal decomposition does occur, whereas alloys outside the spinodal decompose by a discontinuous and non-spontaneous process, i.e. decomposition occurs by nucleation and growth.

1. Introduction

The linear theory of spinodal decomposition, as propounded principally by Cahn [1], predicts periodic and directional composition fluctuations in elastically anisotropic crystals and there has been a tendency to attribute all periodic microstructures to spinodal decomposition. This, however, has aroused controversy, since periodic structures can also be formed by nucleation and growth [2].

To avoid such ambiguity, Rundman and Hilliard [3] suggested using small-angle X-ray scattering (SAXS) to study spinodal decomposition. Results obtained by this technique, however, have not always permitted unambiguous interpretation, as it has been shown [4] that previous notions concerning "proof" of spinodal decomposition by SAXS requires that decomposition be accurately describable by the linear theory.

Recently, more subtle micrographic evidence has been adduced [5, 6] to suggest the occurrence of spinodal decomposition. Sinclair *et al.* [5], using field ion microscopy on Ni–14% Ti specimens, found gradual composition changes at the interface between the decomposition products at the initial stages of decomposition. As ageing time increased, however, the diffuse interface sharpened. Laughlin and Cahn [6] observed continuous phase separation in Cu–Ti alloys, as deduced by a "microstructural sequence" method; increasing strain contrast due to larger composition fluctuations was observed with longer ageing times. Since this occurred at constant wavelength of the composition fluctuations, the diffusion coefficient ($\tilde{D}$) must be negative, which in a binary system must imply the crossing of a spinodal.

In the present work, decomposition of several TiO_2–SnO_2 alloys have been studied using large-angle X-ray diffraction (LAXD), SAXS, transmission electron microscopy (TEM), and electron diffraction. It is shown that alloys within the spinodal decompose by a continuous and spontaneous process, i.e. spinodal decomposition occurs. Alloys outside the spinodal decompose by a discontinuous and non-spontaneous process, i.e. by nucleation and growth. Before describing our results, however, previous work on decomposition of TiO_2–SnO_2 alloys will be briefly reviewed.

2. Review of the literature

At elevated temperatures, TiO_2 (rutile) and SnO_2 (cassiterite) form a continuous solid solution with space group $P4_2/mmm$. Subsolidus phase equilibria in this system was recent redetermined [7], and the miscibility dome was found to be almost symmetrical–the critical composition occurs at 47 ± 2 mol % TiO_2 at a critical temperature of $1430 \pm 5°C$ (Fig. 1). As was first demonstrated by Schultz and Stubican [8, 9], decomposition of equimolar alloys produces composition fluctua-

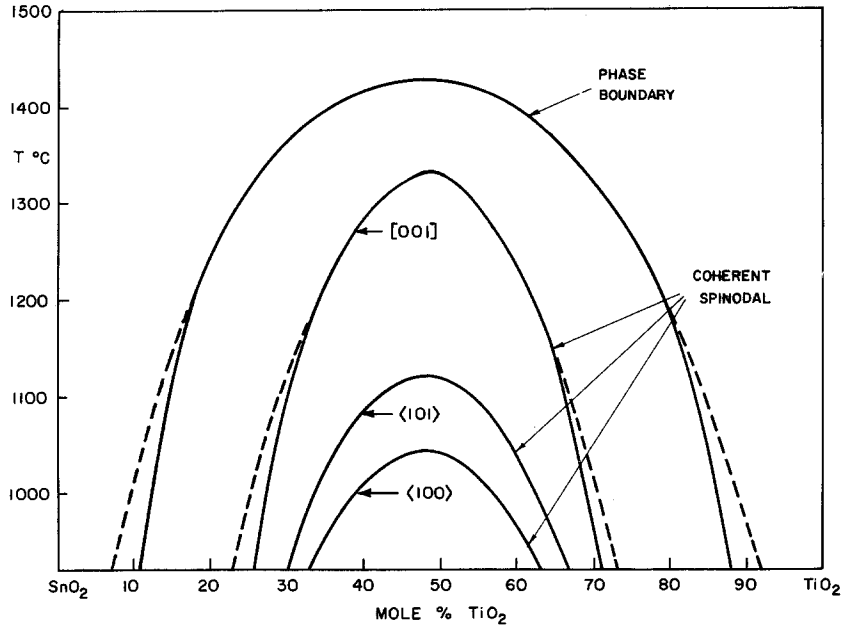

Figure 1 Subsolidus equilibria in the TiO_2–SnO_2 binary. The several spinodals were calculated using the regular solution model. See [7] for further details.

tions along [0 0 1], and the [0 0 1] spinodal was calculated to be depressed by 105°C below the solvus [7].

Schultz and Stubican [8, 9] were the first to study decomposition in the TiO_2–SnO_2 system. They annealed equimolar alloys at 1000 to 1150°C and as already mentioned, observed periodic composition fluctuations along [0 0 1] by TEM. These periodic fluctuations were attributed to decomposition via the spinodal mechanism; in addition, they observed side bands for hkl reflections with $l \neq 0$ by LAXD. The [0 0 1] composition fluctuations were attributed to the anisotropy in elastic free energy, although Wu and Mendelson [10] have more recently pointed out that anisotropies in the diffusion mobility and in the gradient energy can also contribute to the anisotropic decomposition.

Herman and MacCrone [11] have criticized Schultz and Stubican's claim of spinodal decomposition on two counts: (1) observations of modulated structures are not sufficient proof of the spinodal mechanism, and (2) their own (unpublished) SAXS spectra did not show the expected "crossover". Stubican and Schultz [12], in rebuttal, argued that the side bands they observed could only be due to continuous composition fluctuations and that the failure to observe a crossover during SAXS was due to these experiments being performed at a late stage of decomposition. However, Hargreaves [13] and Guinier [14] have argued that discontinuous composition fluctuations can also lead to side bands, and our previous analysis [4] showed that the lack of a crossover is inconsistent with a linear theory but not with the spinodal mechanism in general. The criticism of late stage decomposition is well taken but also applies to the TEM observations in question, since the results to be presented below show that decomposition occurs at much earlier times and lower temperatures than were used by Schultz and Stubican.

Finally, it was observed that the wavelength of the composition fluctuations receiving maximum amplification first decreased with annealing time, reached a minimum, and then increased [8]. Gupta and Cooper [15] simulated the kinetics of spinodal decomposition of a 40 mol % TiO_2 alloy. Their one-dimensional numerical solution of the diffusion equation for spinodal decomposition suggested that spinodal decomposition could explain the entire process of the wavelength changes with annealing time.

In summary, it is clear that the question of spinodal decomposition in TiO_2–SnO_2 alloys is controversial, in part because no studies have been conducted during the *initial* stages of decomposition. The present work attempts to resolve these difficulties.

3. Experimental procedures and results

3.1. Experimental procedures

Alloys containing 20, 50 and 80% TiO_2 were prepared by homogeneously mixing SnO_2* and TiO_2† powder and hot-pressing at 1450°C into cylinders, ~1 cm diameter by ~1 cm long, using a Poco graphite die, a 99.9% alumina tube as a liner (to prevent reaction with the graphite) and alumina plungers. Specimens were sliced into ~1 mm thick discs in a precision wafering machine and solution-annealed at 1580°C for 24h in a well-covered alumina crucible; to minimize evaporation problems, the discs were embedded in previously homogenized single-phase powder of the same composition; they were finally quenched into water. Specimen homogeneity was considered adequate if the half-width of the (2 1 1) LAXD peak was the same as that of pure SnO_2. Decomposition was achieved by annealing in air for various times at various temperatures. Because of the short duration of some annealing experiments, all specimens were inserted into a heated furnace and air-quenched at the completion of the run. (The more modest cooling rate of air-quenching was used to prevent propagation of the cracks introduced during the water-quenching from the homogenization temperature.)

For the LAXD studies, a conventional X-ray diffractometer was used with Ni-filtered Cu$K\alpha$ radiation; no attempt was made to resolve the Cu$K\alpha_1$, Cu$K\alpha_2$ doublet. Attention was focused on the (2 1 1) peak.

For TEM studies, specimens were mounted on a glass slide, ground using abrasive paper to about half the initial thickness, and polished with 3 μm diamond paste; after removal from the glass slide, they were remounted up-side down in a 15 μm etch-well in a glass slide and ground until the specimen was flush with the glass surface. Performation to ensure electron transparency in a 650 kV Hitachi microscope was performed using ion thinning [16].

Specimen preparation for SAXS was similar but more tedious, because the need for specimen integrity was greater. One side of the specimen was ground, and the small cracks present were sealed with epoxy. After the epoxy set, the specimens were glued up-side down in a 24 μm etch-well in a glass slide, and ground until the surface was even with the glass slide. (X-ray spectra from two specimens prepared with and without epoxy were identical.) The 3 to 4 mm specimen was then mounted at the centre of a hole in a lead plate, which itself was mounted in a lead plate holder, and the specimen assembly was fixed in the small-angle X-ray bench of a Rigaku–Denki high intensity, rotating anode unit. A 1.0 mm diameter X-ray beam, collimated by two pinholes of 0.5 and 0.3 mm, passed through the centre of the specimen and a 180 or 250 mm specimen–film distance was employed. Identical exposures of 27h at 46 kVA accelerating voltage and 70 mA beam current were used; films were used instead of a counter because of the low diffracted X-ray intensity. Plots of relative intensity versus radial position (equivalent to diffraction angle) were made using a Joyce–Lobell microdensitometer. (Further experimental details will be given in Section 3.4)

*99.6% Purity, Fisher Scientific Co, Pittsburgh, Pa, USA.
†99.9% Purity, Fisher Scientific Co, Pittsburgh, Pa, USA.

3.2. LAXD results

LAXD decomposition studies of the three alloys studied are shown in Figs. 2 to 4. The equimolar alloy, the only one lying within the spinodal, will be discussed first.

The (2 1 1) peak of a single phase specimen and specimens annealed at 900°C for 6, 9, 15, 20 and 60 min are shown in Fig. 2a and b; Fig. 2c shows the pattern for a specimen annealed for 7.5h at this temperature. As can be seen, the diffraction peak of the single phase specimen is symmetrical and the peak itself is quite narrow. Upon annealing, appreciable scattered intensity, i.e. side bands, is observed in addition to the main diffraction peak, with the intensity being greater on the low angle side of the diffraction peak. After annealing for 20 min, a distinct hump is observed on the low-angle side and a similar second peak is observed on the high-angle side after annealing for 1h. Three distinct peaks are observed from the specimen annealed for 7.5h.

Following de Fontaine [17], the asymmetry shown in Fig. 2 is attributed to modulations in both the lattice parameters and the atomic scattering factors. The central peak in Fig. 2c, of course, is due to diffraction from the "residual" undecomposed matrix.

Fig. 3 shows the results of a similar experiment for the 80% TiO_2 alloy annealed for times up to 116h at 1160°C, while Fig. 4 shows the 20% TiO_2 alloy annealed for times up to 456h at this

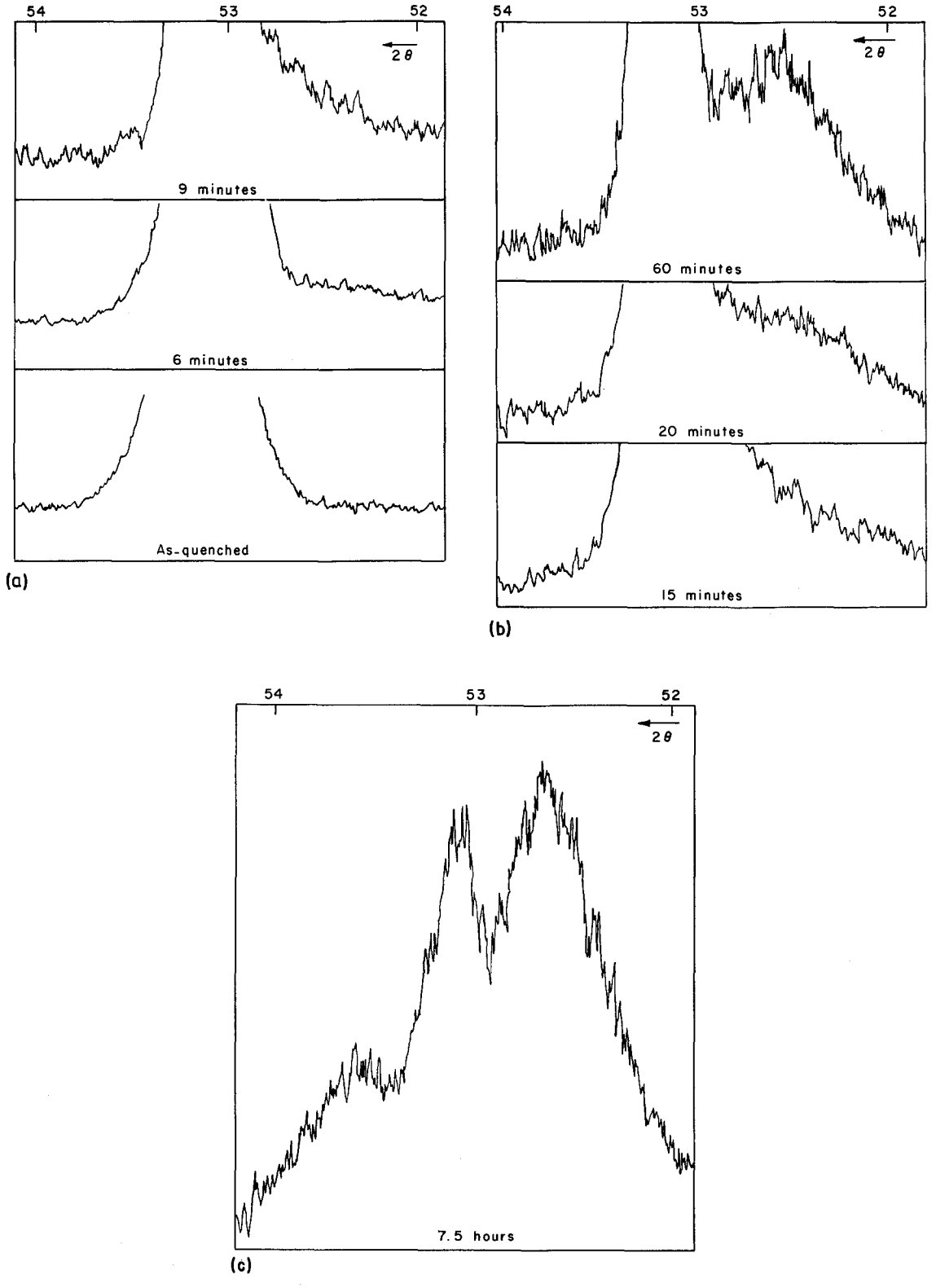

Figure 2 (2 1 1) X-ray diffraction peaks of the equimolar alloy. (a) As-quenched samples and those annealed at 900° C for 6 and 9 min; (b) the diffraction peak of samples annealed for 15, 20 and 60 min; (c) the peak for the sample annealed for 7.5 h.

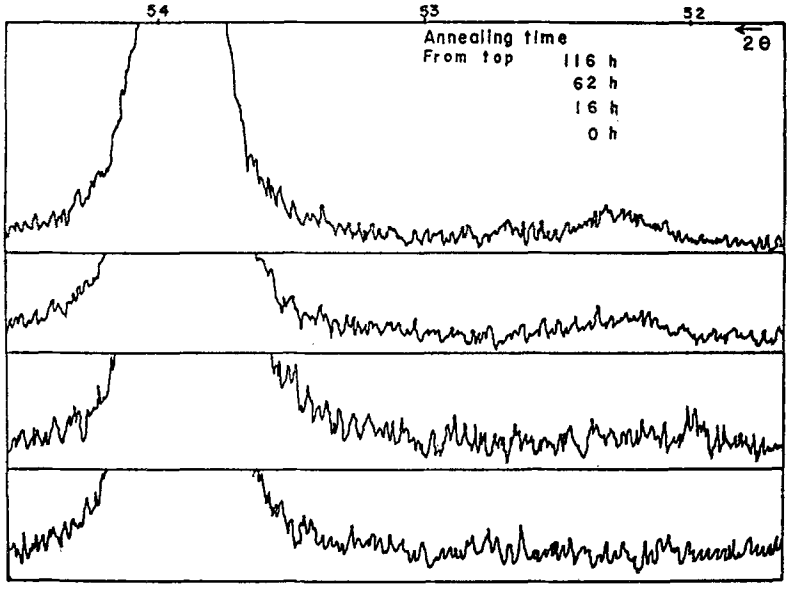

Figure 3 (2 1 1) X-ray diffraction peak for 80 mol% TiO_2–20 mol% SnO_2 alloy annealed at 1160° C for times up to 116 h.

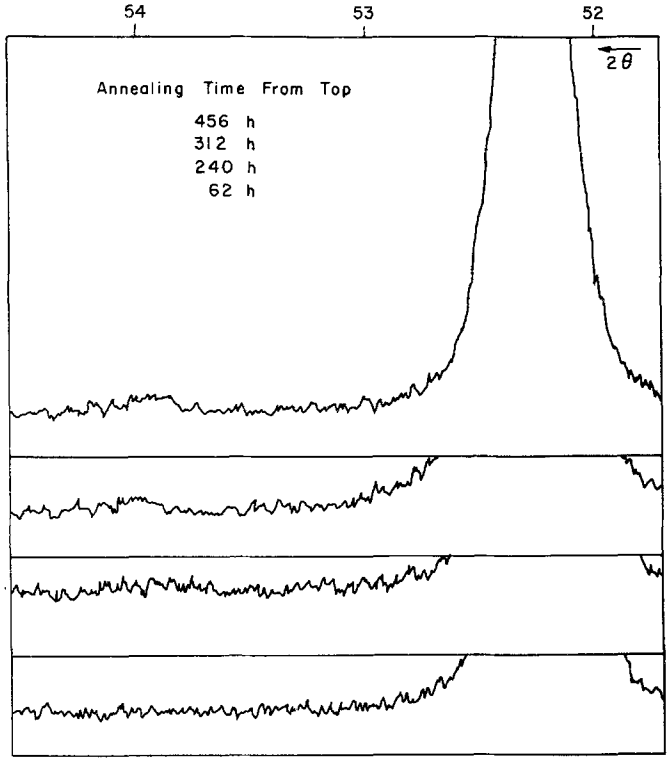

Figure 4 (2 1 1) X-ray diffraction peak for 20 mol% TiO_2–80 mol% SnO_2 alloy annealed at 1160° C for times up to 456 h.

temperature. (Note that both these compositions are in the "metastable" portion of the phase diagram at this decomposition temperature.) In both cases, the shape of the original (2 1 1) X-ray peak is unchanged throughout the annealing; the new (2 1 1) peak appears well-developed above the background and well-separated from the main peak. Since the precipitate causing the new peak in Fig. 3 is SnO_2-rich, the higher scattering factor of Sn allows this peak to be observed at shorter

annealing times than is the case for the TiO_2-rich precipitate in Fig. 4.

3.3. TEM results

For the TEM study, single phase specimens of the equimolar composition were annealed at temperatures of 750 to 1000° C, while one 80% TiO_2 sample was annealed at 900° C.

Fig. 5a shows a micrograph of the equimolar single phase alloy, while Fig. 5b and c show samples annealed at 750° C for 10 and 20 min, respectively. The fine structure visible in the latter two micrographs are attributed to the initial stages of decomposition. The sidebands visible in the diffraction pattern of the latter sample (inset to Fig. 5c) is further evidence of decomposition.

The microstructural evolution for this alloy upon further decomposition is shown in the sequence depicted in Fig. 6. The annealing temperature was 900° C, and annealing times from 6 min to 127 h were used.

Well-defined and periodic decomposition products are maintained for the entire annealing sequence; in all cases, the direction of spot separation in diffraction patterns is parallel to [0 0 1]. This spot sepration allows a calculation of the lattice parameter difference of the two exsolved phases. From Bragg's law, it is easily derived that

$$\Delta c = \frac{-c^3}{l^2}\frac{R\Delta R}{(\lambda L)^2} = \frac{-c^3}{l^2 d^2}\frac{\Delta R}{R}, \qquad (1)$$

where R is the distance from the (0 0 0) spot to the original ($h\,k\,l$) diffraction spot in reciprocal space, ΔR is the spot splitting, λ is the wavelength of 650 kV electrons, and L is the camera length of the electron microscope. The data for Fig. 6f are shown in Table I; the mean Δc is 0.215 Å.

The phase boundary compositions at 900° C are 10.5% TiO_2 and 80 mol % TiO_2, as estimated from Fig. 1; the corresponding lattice parameter difference, Δc, (taken from [7]) is 0.1790 Å, in tolerable agreement with experiment.

TABLE I

Index	R(cm)	ΔR(cm)	d(Å)	Δc(Å)
$(\bar{2}\,\bar{2}\,4)$	2.205	0.14	0.6973	0.2432
$(\bar{1}\,\bar{1}\,3)$	1.595	0.095	0.9795	0.2009
$(1\,1\,\bar{5})$	2.58	0.17	0.6049	0.2098
(0 0 2)	1.02	0.08	1.5383	0.2413
$(1\,1\,\bar{4})$	2.09	0.12	0.7491	0.1863
$(1\,1\,\bar{3})$	1.60	0.10	0.9795	0.2108

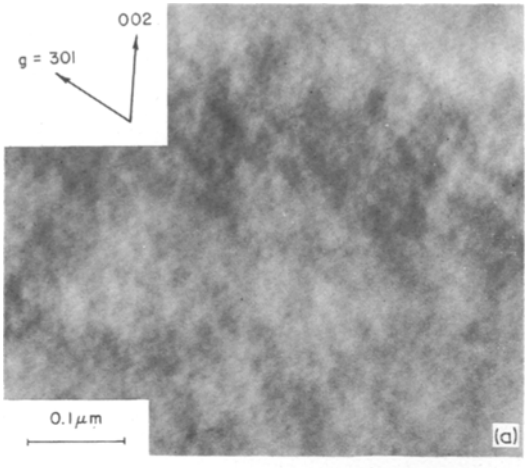

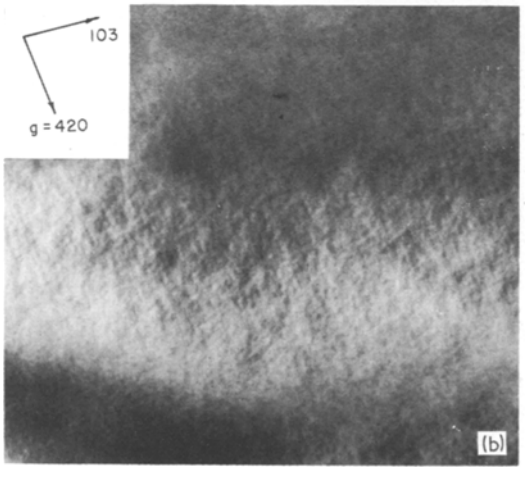

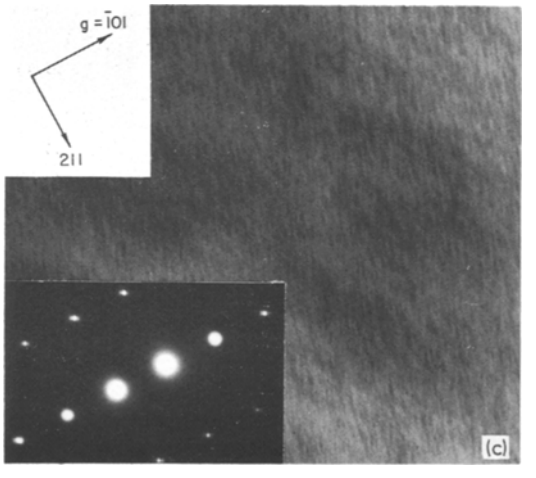

Figure 5 TEM evidence of the earliest stages of decomposition of the equimolar alloy. (a) As-quenched sample; (b) and (c) samples annealed at 10 and 20 min, respectively, at 750° C. Note the side bands adjacent to diffraction spots in the electron diffraction inset to (c). Magnifications for (b) and (c) as for (a).

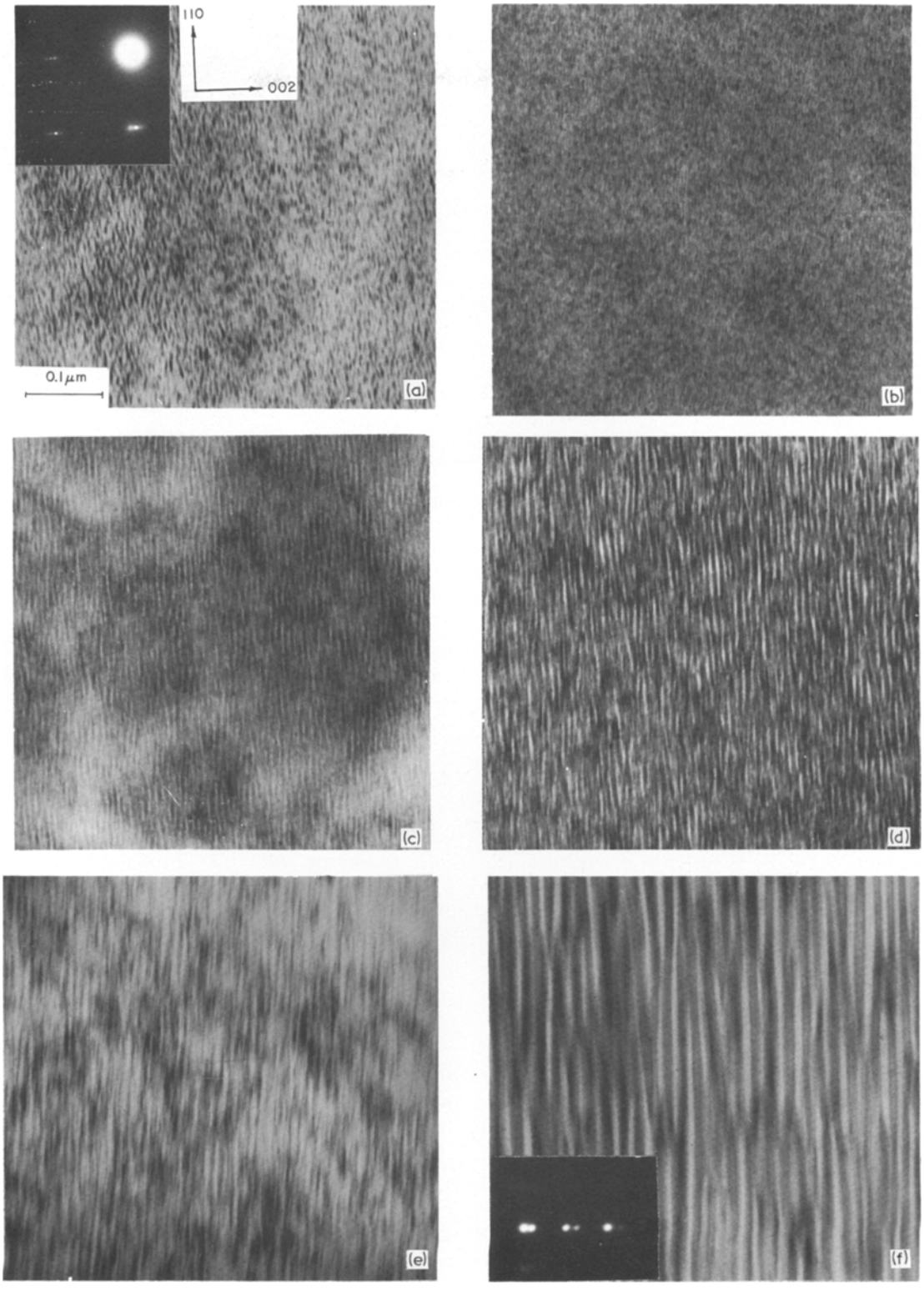

Figure 6 Microstructural evolution of the equimolar alloy decomposed at 900° C. The annealing times for (a) to (f) are 6, 15, 20, 60 and 450 min, and 127 h, respectively. All magnifications and orientations as for (a).

Figure 7 Electron micrograph of the most extensively decomposed equimolar alloy studied, which was annealed for 63 h at 1000° C. See text for further discussion.

The most extensively decomposed specimen studied by TEM was annealed for 63 h at 1000° C and is shown in Fig. 7. The characteristic lamellar periodicity is no longer perfectly defined and the presence of two sets of spots in the diffraction pattern makes indexing very difficult. (The indexing shown in Fig. 7 refers to only one set of spots.)

The nature of the decomposition products of the 80% TiO_2 alloy annealed at 900° C for 15 h is shown in Fig. 8. No periodic precipitates were found, nor was spot separation observed. However, extensive precipitation was observed at high-angle grain boundaries, as shown in Fig. 8a and b. Consider Fig. 8a first. As can be seen, the two grains have quite different orientations – their zone axes are $[1\ \bar{1}\ \bar{1}]$ and $[1\ \bar{1}\ \bar{2}]$ – so that the misorientation is $\sim 18°$. When the selected-area diffraction aperature included the grain-boundary region, the diffraction pattern consisted of a superposition of the individual diffraction patterns of the two grains, but with each diffraction spot showing clear spot separation. This indicates that the presence of the grain boundary caused heterogeneous precipitation, the precipitate phase having a well-defined orientation relationship with the matrix on either side of the grain boundary. The grain-boundary precipitate itself can be more clearly seen in Fig. 8b. As with the equimolar alloy, the observed spot separation can be used to calculate the lattice parameter difference between the precipitate and matrix. The new diffraction spots have appeared along [0 0 1] close to the original spot but with a larger d spacing, consistent with it being SnO_2-rich. Equation 1 is still used, but ΔR is now the distance from the original $(h\ k\ l)$ spot to the new precipitate spot. Using the spot separations for the $(\bar{3}\ 0\ \bar{3})$, $(\bar{4}\ 0\ \bar{4})$, and $(5\ 1\ 4)$ reflections, Δc was found to be 0.179, 0.169, and 0.223 Å, respectively, again in reasonable agreement with the expected value of 0.179 Å.

3.4. SAXS results

SAXS studies of the equimolar composition were conducted at 900° C; a typical scattering pattern and its microdensitometer scan are shown in Fig. 9a and b, respectively, while the results of the annealing experiments themselves, in the form of scattered intensity (I) versus wave number (β) curves, are shown in Fig. 10.

The SAXS diffraction pattern (Fig. 9a) is somewhat unusual and requires further comment. The pattern contains several radially elongated streaks and not a ring pattern. Since the diffraction is occurring from a lamellar structure (cf. Fig. 6), the usual Bragg equation, $\lambda = 2d \sin \theta$, describes the small-angle X-ray scattering, with the spacing d being ~ 100 Å, and the diffraction angle $\theta \sim 0.5°$. Since the scattered intensity was so low, unfiltered

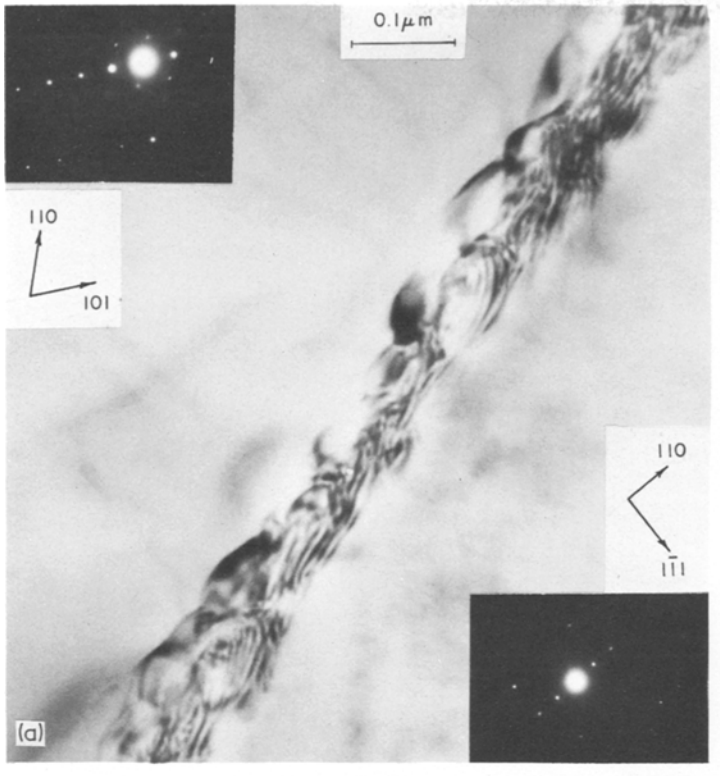

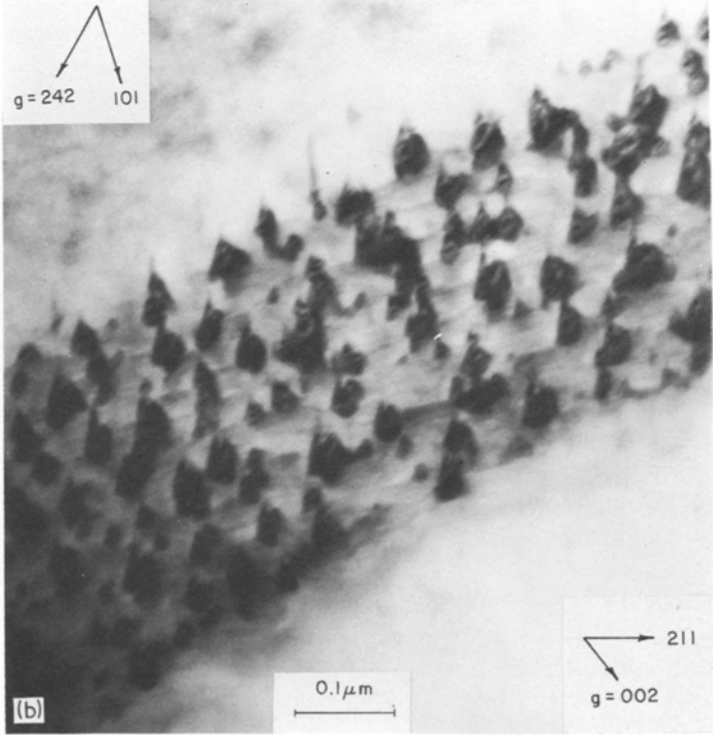

Figure 8 TEM evidence of grain-boundary precipitation in an 80 mol% TiO_2–20 mol% SnO_2 specimen annealed at 900° C for 15 h. (a) and (b) examples of two different high-angle grain boundaries. The misorientation is 18° in (a) and 68° in (b).

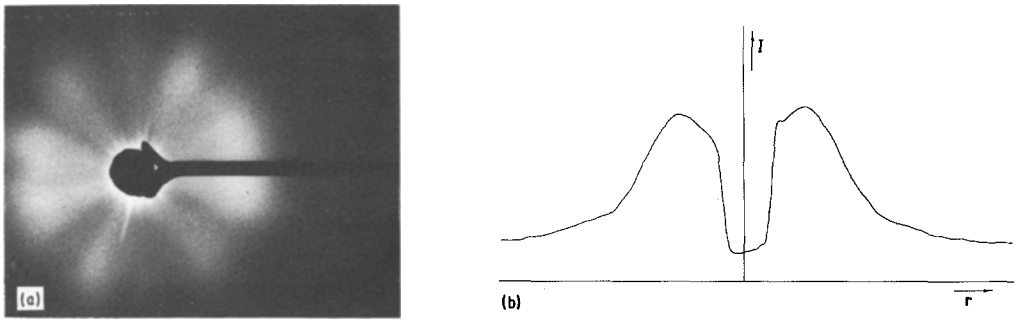

Figure 9 (a) Small-angle X-ray diffraction pattern and (b) corresponding microdensitometer scan for an equimolar sample annealed at 900° C for 20 minutes.

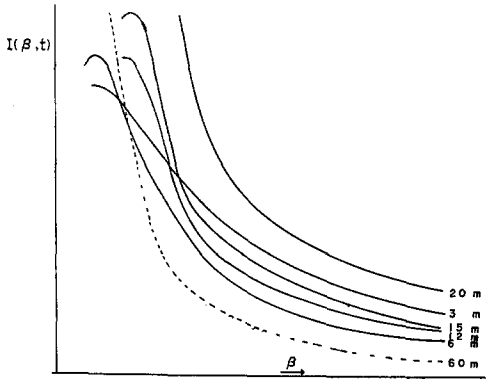

Figure 10 I–β curves derived from small-angle X-ray scattering data for samples annealed at various times at 900° C.

Cu radiation was used, with β being calculated assuming the diffraction occurred for the Cu$K\alpha$ radiation.*

Given the small diffraction angles, the lamella planes that are diffracting must be nearly parallel to the X-ray beam. The lamella planes are not perfectly oriented, however, and there are small angular deviations in all directions within the plane perpendicular to the c-axis. Thus, a streak that is symmetric around the X-ray beam is expected, i.e. a single grain with lamella planes almost parallel to the X-ray beam gives rise to two radially elongated streaks. If the number of grains satisfying the diffraction condition is large enough to give diffraction in all directions, a diffraction ring centred at the central X-ray beam will be observed. In the present experiments, while the orientation of the grains is random, the number of grains exposed to the X-ray beam is small and a simple calculation indicates that the number of grains satisfying the diffraction condition, i.e. with the c-axis within 1° about any direction perpendicular to the X-ray beam, is of the same order as the number of streaks observed in Fig. 9a. Since the centre of the X-ray beam could not be accurately located, the microdensitometer was used to scan only symmetrical pairs of streaks, and the centre of the X-ray beam was located at the centre of the two maxima in the spectra.

4. Discussion

It is clear, particularly from the LAXD and TEM results, that alloys inside and outside the spinodal decompose differently. For the 20 and 80% TiO_2 alloys in the metastable portion of the phase diagram, classical heterogeneous nucleation and growth appears to occur. The longer times needed to observe detectable decomposition, compared to the equimolar alloy, is due to the need to form nuclei of a critical size which have a large composition difference from that of the matrix; of course, this is also the reason why the precipitate peaks are well separated from the main peak in LAXD. The fact that no noticeable changes occurred in the shape of the main diffraction peak, and the small intensity of the precipitate peak, result from the small precipitate volume fraction in these alloys.

Decomposition of the equimolar alloy at temperatures $\leqslant$ 1000° C would be expected to occur spinodally, and all our evidence is consistent with this. The lack of any incubation period (see Figs.

*Sin $2\theta = R/L \cong 2\theta$, where R is the distance from the central X-ray beam to the position of maximum diffracted intensity on the X-ray film and L is the specimen-to-film distance. The diffraction equation can, therefore, be written $R = \lambda L/d$. For d = 100 Å and L = 250 mm, R for Cu$K\beta$ radiation would be 7% less than R for Cu$K\alpha$ radiation. Since the intensity of the $K\beta$ radiation is $\sim \frac{1}{2}$ that of $K\alpha$, this effect was ignored.

2, 5 and 10) indicates that decomposition occurs continuously and spontaneously. In the LAXD study (Fig. 2), the composition fluctuations, which cause the side band intensity, are seen to increase gradually in magnitude with increased annealing time and also to cause a gradual increase (decrease) in the TiO_2-poor (-rich) decomposition product.

In electron transmission, evidence of decomposition can be seen uniformly throughout the grains in the bright-field micrograph for annealing times as short as 10 min at 750° C (Fig. 5b) and sidebands around diffraction spots are visible in the diffraction pattern of the 20 min specimen (inset to Fig. 5c).

Although the SAXS spectra (Fig. 10) do not show the "crossover" often taken as "proof" of spinodal decomposition, our previous analysis [4] has shown that such a crossover is only expected if the decomposition can be described by a linear spinodal theory. We believe that crossovers are likely to be observed only in samples "perfectly" quenched from very high temperatures (this would be indicated by a "flat" I–β curve, i.e. one where the scattered intensity is essentially independent of wave number), and such a good quenching could not be achieved in the present experiments.

It finally remains to discuss the magnitude of the composition fluctuations and their variation with annealing time. The most straightforward way is to use the SAXS data. The wave number receiving maximum amplification is readily apparent from data such as is shown in Fig. 10, and this characteristic periodicity is given in Table II as a function of annealing time at 900° C. As seen in Fig. 6, electron micrographs of samples decomposed at this temperature showed periodically arrayed lines of contrast perpendicular to [0 0 1]. Even though strain contrast due to precipitates in electron microscopy is complicated and in some cases is not in the same orientation as the particles causing the strain [18], it is clear in the present study that the periodic contrast in the micrographs was caused by a periodic strain between two phases, differing alternatively in composition and in lattice parameter along [0 0 1]. The TEM data are also shown in Table II, and are in substantial agreement with the SAXS data; they are based on the assumption that the dark lines in the micrographs are due to strain contrast; the characteristic periodicity was thus calculated to be twice the distance between adjacent dark lines.

TABLE II

Annealing time at 900° C (min)	Direct Observation* (Å)	Optical Diffraction (Å)†	SAXS (Å)
6	144	138	133
9	133	–	124
15	88	–	77
20	154	164	157
60	180	208	193
450	233	256	213
7620	417		

*In order to measure the periodicity by transmission electron microscopy only grains oriented such that [0 0 1] was perpendicular to the electron beam were used. All micrographs were taken at × 50 000. The plates were then magnified × 4 and projected onto a screen to measure the characteristic periodicities.

†Since the periodicity of the structures were not perfect, the characteristic spacings were measured using an optical diffractometer (6328 Å laser and a 178.1 cm camera length). Because of the imperfect periodicity, only diffraction up to second order could be recorded.

In agreement with Schultz and Stubican's data [8] and Gupta and Cooper's calculation [15], Table II shows that the characteristic periodicity first decreases with ageing time to a minimum and then increases. Following Gupta and Cooper, we attribute this to the need for the composition fluctuations formed during the imperfect quenching to decay, before coarsening begins. For the 900° C annealing experiments, insufficient data are available at large wave numbers of the composition fluctuation to establish whether $t^{1/3}$ coarsening occurs; however, such behaviour is found for a "quenched" sample containing a composition fluctuation of 150 Å and annealed at 1000° C (these data are reported elsewhere [19]).

Acknowledgments

We acknowledge useful conversations with A. R. Cooper. This work was supported by the U.S. Army Research Office, Durham, N.C., under Grant No. AROD 3112473G95.

References

1. J. W. CAHN, *Trans. Met. Soc. AIME* **242** (1968) 166.
2. A. J. ARDELL and R. B. NICHOLSON, *Acta Met.* **14** (1966) 1295.
3. K. B. RUNDMAN and J. E. HILLIARD, *ibid* **15** (1967) 1025.

4. M. W. PARK, A. R. COOPER and A. H. HEUER, *Scripta Met.* **9** (1975) 321.
5. R. SINCLAIR, J. A. LEAKE and B. RALPH, *Phys. Stat. Sol. (a)* **26** (1974) 285.
6. D. E. LAUGHLIN and J. W. CAHN, *Acta Met.* **23** (1975) 329.
7. M. W. PARK, T. E. MITCHELL and A. H. HEUER, *J. Amer. Ceram. Soc.* **58** (1975) 43.
8. A. H. SCHULTZ and V. S. STUBICAN, *Phil. Mag.* **18** (1968) 929.
9. V. S. STUBICAN and A. H. SCHULTZ, *J. Amer. Ceram. Soc.* **53** (1970) 211.
10. K. WU and K. S. MENDELSON, *J. Chem. Phys.* **58** (1973) 2929.
11. H. HERMAN and R. K. MACCRONE, *J. Amer. Ceram. Soc.* **55** (1972) 50.
12. A. H. SCHULTZ and V. S. STUBICAN, *ibid* **55** (1972) 50.
13. M. E. HARGREAVES, *Acta Cryst.* **4** (1951) 301.
14. A. GUINIER, *Acta Met.* **3** (1951) 510.
15. P. K. GUPTA and A. R. COOPER, *Phil. Mag.* **21** (1970) 611.
16. A. H. HEUER, R. F. FIRESTONE, J. D. SNOW, H. W. GREEN, R. G. HOWE and J. M. CHRISTIE, *R. Sci. Inst.* **42** (1971) 1177.
17. D. DE FONTAINE, in "Local Atomic Arrangements Studied by X-ray Diffraction", edited by J. B. Cohen and J. E. Hilliard (Gordon and Breach, New York, 1966) p. 51.
18. P. J. FILLINGHAM, H. J. LEAMY and L. E. TANNER, "Electron Microscopy and Structure of Materials", edited by G. Thomas, R.M. Fulrath and R.M. Fisher (University of California Press, Berkeley, 1972) p. 163.
19. M. W. PARK, T. E. MITCHELL and A. H. HEUER, in "Application of Transmission Electron Microscopy to Mineralogy", edited by H. R. Wenk, P. E. Champness, J. M. Christie, J. M. Cowley, A. H. Heuer, G. Thomas, and N.J. Tighe (Springer–Verlag, Berlin, 1976) p. 205.

Received 29 December 1975 and accepted 15 January 1976.